Franck-Condon higher order lattice excitations in the $LaFe_{1-x}Cr_xO_3$ ($x=0$, 0.1, 0.5, 0.9, 1.0) perovskites due to Fe-Cr charge transfer effects

Jakob Andreasson, Joakim Holmlund, Christopher S. Knee, Mikael Käll, and Lars Börjesson
Department of Applied Physics, Chalmers University of Technology, SE-41296 Göteborg, Sweden

Stefan Naler, Joakim Bäckström,* and Michael Rübhausen
Institut für Angewandte Physik, Universität Hamburg, Jungiusstrasse 9, D-20355 Hamburg, Germany

Abul Kalam Azad† and Sten-G. Eriksson‡
Studsvik Neutron Research Laboratory, Uppsala University, 61182 Nyköping, Sweden
and Department of Inorganic Chemistry, Göteborg University, 41296 Göteborg, Sweden
(Received 31 May 2006; revised manuscript received 22 December 2006; published 9 March 2007)

First and higher order lattice excitations in the *B*-site disordered perovskites $LaFe_{1-x}Cr_xO_3$ ($x=0$, 0.1, 0.5, 0.9, and 1) and $La_{0.835}Sr_{0.165}Fe_{0.5}Cr_{0.5}O_{3-\delta}$ are investigated using temperature dependent and polarized inelastic light scattering [$\lambda=515$ nm (2.41 eV) and 676 nm (1.83 eV)] on oriented crystallites. A peak at approximately 2.4 eV in the imaginary part of the dielectric function of $LaFe_{0.5}Cr_{0.5}O_3$ is assigned to a charge transfer from Fe^{3+} (d^5) to Cr^{3+} (d^3) ions, coupled with the appearance of an intense A_g-like mode at approximately 700 cm^{-1} in the Raman data. This excitation is identified as a symmetric oxygen breathing mode activated by the Fe-Cr charge transfer through an orbital coupling mechanism. Higher order scattering (up to seventh order) of the intrinsic Raman active symmetric breathing mode is also explained by an orbital-mediated electron-phonon coupling, similar to the Franck-Condon effect observed in the Jahn-Teller active-perovskite-structured manganite $LaMaO_3$. These results show that the Franck-Condon mechanism is a more common mechanism for resonant higher order scattering in solids than previously believed and propose the $LaFe_{1-x}Cr_xO_3$ system as a model system for electron-phonon coupling and higher order Raman scattering in solids.

DOI: 10.1103/PhysRevB.75.104302 PACS number(s): 63.20.Kr, 78.30.−j, 63.50.+x

I. INTRODUCTION

The ABO_3 perovskite structure is among the most versatile crystal structures in oxide research. Compounds with variations of the simple perovskite structure exhibit an astonishing variety of exotic magnetic and electronic behavior, such as high-temperature superconductivity,[1] collosal magnetoresistance[2] (CMR), and half-metallicity.[3] Intense research efforts have shown the importance of the coupling between the transition-metal (TM) *d* orbitals and the oxygen lattice for the complex properties present in these materials, in particular, for the CMR effect in $La_{1-x}Sr_xMnO_3$.[4–6] Recently, the discovery of half-metallicity in the ferrimagnetic (FiM) compound Sr_2FeMoO_6 has increased the interest in compounds with *B*-site-ordered double perovskite (DP) lattices.[7]

The ideal perovskite oxide can be visualized as having a *B*-site transition-metal ion (2+, 3+, and 4+) located in the center of a symmetric oxygen octahedron that, in turn, is embedded in an *A*-site ion cube. However, most real perovskites display symmetry breaking due to displacements of the crystallographic sites from the ideal cubic positions. Such lowering of symmetry is often accompanied by the appearance of Raman-active phonons.

The influence of the electronic configuration and orbital ordering on the Raman spectra of these distorted perovskites has been addressed through theory.[8,9] Within the manganite family, it has been predicted that orbitons can be excited in orbitally ordered $LaMnO_3$, in which the Mn ions have a Jahn-Teller (JT) active d^4 electronic configuration.[4,10] Further, the electronic configuration of JT active perovskites has led to the prediction, through local-spin density-functional theory calculations,[11] of a Franck-Condon (FC) effect manifested through an increase of the higher order phonon Raman cross section.

FC multiphonon bands are well established in small molecules, where altered atomic coordinates generally follow from electronic excitations.[12] On the contrary, in solids, electronic excitations quickly delocalize and a trapping mechanism is needed for a FC effect to occur. This type of behavior has only recently been discovered in TM oxides of perovskite and perovskitelike structures and is believed to be quite rare. The available data mostly concern the manganites and studies on other materials are scarce.

Raman studies have been carried out on manganites, such as $LaMnO_3$, in search of orbitons and FC-induced higher order scattering. Claims of direct observations of orbitons have been made,[13] but the interpretation has been questioned by many authors[14–16] who have instead assigned the observed peaks to second order phonon excitations enhanced through a FC-induced resonance.[15,16] However, both the first and higher order scatterings in $LaMnO_3$ consist of several (at least 4) partially overlapping peaks with a complex temperature and polarization dependence, making the exact assignment of all the higher order features difficult and controversial.[17,18] In other studies of similar compounds such as the Ruddlesden-Popper $R_{2-2x}Sr_{1+2x}Mn_2O_7$, R=La, Pr, Nd, and Dy phases, the higher order excitations do not show any unexpected resonance behavior.[19] Recently, claims have also been made of observations of FC modes in the ordered DP Sr_2MnWO_6.[20]

In this work, we study the complex interplay between the lattice and the electronic dynamics in the *B*-site-disordered $LaFe_{1-x}Cr_xO_3$ ($x=0$, 0.1, 0.5, 0.9, and 1) and $La_{0.835}Sr_{0.165}Fe_{0.5}Cr_{0.5}O_{3-\delta}$ perovskites. The remarkable intensity of the first and higher orders of a symmetric breathing mode in the mixed *B*-site compounds is explained by connecting a light-induced CT from the Fe to the Cr ions to the lattice dynamics through a strong coupling between the oxygen *p* orbitals and the TM *d* orbitals.

II. EXPERIMENT

The polycrystalline samples were made by a solid-state sintering method and a phase purity confirmed by powder x-ray diffraction. The structural and magnetic properties of $LaFe_{0.5}Cr_{0.5}O_3$ have been throughly investigated using a range of techniques.[21]

The $LaFe_{1-x}Cr_xO_3$ and $La_{0.835}Sr_{0.165}Fe_{0.5}Cr_{0.5}O_{3-\delta}$ (Ref. 22) samples adopt a pseudocubic structure of orthorhombic symmetry described by the space-group *Pbnm*, a nonstandard setting (short *a* and *b* axes and long *c* axis) of the *Pnma* (D_{2h}^{16}, No. 62) space group (short *a* and *c* axes and long *b* axis). Below, a notation corresponding to the *Pnma* setting is used. Accordingly, vibrational modes of A_g and B_{2g} symmetries are excitable in the *ac* plane.[23,24] (For the relations between Raman activity in the *Pnma* and *Pbnm* settings see Ref. 25.) There are no structural phase transitions predicted in the temperature interval of this study, but electron diffraction and high-resolution transmission electron microscopy[21] (HRTEM) of the crystallographic *ac* plane indicate the presence of domains of different orientations. This microtwinning makes the *a* and *c* directions indistinguishable on the scale of the laser spot, causing the Raman spectra to represent an average scattering from the *a* and *c* directions.

Individual single crystallites are identifiable in the $x=0$, 0.1, 0.5, and $La_{0.835}Sr_{0.165}Fe_{0.5}Cr_{0.5}O_{3-\delta}$ compounds, while the $x=0.9$ and $x=1$ compounds are fine powders. Due to the strong *B*–O bonds in ABO_3 perovskite structures, as-grown crystallite surfaces mainly represent the crystallographic *ac* planes.[23] The surfaces selected for the polarized scattering study were approximately $5\times5-10\times10$ μm^2 and displayed straight edges representing the *a* or *c* crystallographic axes used for orientation. For the temperature study on the $LaFe_{0.5}Cr_{0.5}O_3$ compound, the edges were aligned with the x' and z' polarization directions of the setup, where primes indicate rotation by 45° (Fig. 1). In the Porto notation, with polarization vectors x', y, and z' coinciding with the crystallographic *a*, *b*, and *c* axes, the selection rules in the *ac* plane for the space-group *Pnma*, in backscattering geometry, are[23] $y(xx/zz)\bar{y}\rightarrow A_g$, $y(xz/zx)\bar{y}\rightarrow B_{2g}$, $y(x'x'/z'z')\bar{y}\rightarrow A_g+B_{2g}$, and $y(x'z'/z'x')\bar{y}\rightarrow A_g$ (weak). The intensity relations of the observed peaks confirm that the scattering configurations used are $x'x'/z'z'$ for parallel and $x'z'/z'x'$ for cross polarized lights.

All spectra were recorded using a DILOR-XY800 spectrometer combined with a notch filter in the single-grating mode (600 or 1800 grooves/mm). The laser was focused onto the sample using a microscope setup with a 40× magnification glass-compensating objective. A spot size of approximately 2 μm was used, allowing the study of individual crystallites of the $x=0$, 0.1, 0.5, and $La_{0.835}Sr_{0.165}Fe_{0.5}Cr_{0.5}O_{3-\delta}$ compounds. For the temperature study, the $x=0.5$ sample was mounted in a CryoVac microcryostat, cooled with liquid He or N_2. The beam power was kept at 1 mW outside the cryostat.

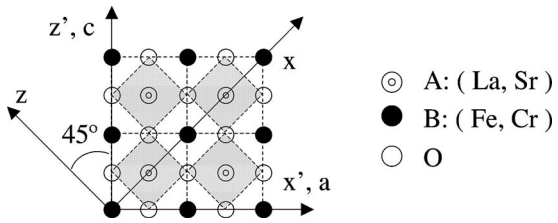

FIG. 1. Crystal axes and polarization directions of an oriented ideal perovskite *ac* plane. Straight edges in as-grown samples run along the *a* and *c* crystal axes due to strong *B*–O bonds and are used for orientation. The white areas represent the oxygen octahedra in the *ac* planes. (Note that the *A* sites are not in the same plane as the *B* and O sites).

The excitation wavelengths used were $\lambda=515$ nm (2.41 eV) and 676 nm (1.83 eV) from an Ar^+/Kr^+ laser. All scattered signals were recorded using a liquid-nitrogen-cooled charge-coupled device CCD camera. If nothing else is mentioned in the caption, the spectra presented in each figure are measured in sequence using the same spectrometer settings, normalized to the same incident power and integration time and can be directly compared. All spectra presented have been compensated for the thermal Bose-Einstein factor and are shown with offsets for clarity. The intensities obtained using different wavelengths are normalized using nonresonant (in the visible region) BaF_2 to adjust for spectrometer response and a Raman correction function obtained from the ellipsometry data to adjust for sample properties, such as optical penetration depth. During the course of this investigation, several different spectrometer settings, power densities, and integration times have been used with no significant change in the general appearance of the data.

The ellipsometry measurements, yielding the dielectric function and the Raman correction function, were performed on a polished sample of $LaFe_{0.5}Cr_{0.5}O_3$ using an extended Sentech SE850 spectral ellipsometer covering the spectral range from 0.5 to 5.5 eV. A xenon gas discharge lamp (ultraviolet-visible) and a halogen lamp (near infrared) were used as light sources. In the visible spectral range, the spectral resolution is achived with a single-grating spectrograph equipped with a diode-array detector. In the near-infrared range, a Fourier transform spectrometer was used. The sample was measured in air with an angle of incidence of 70°. The setup is located in a clean room with controlled temperature ($T=20.0\pm0.5$ °C) and relative humidity of $40\%\pm3\%$.

III. RESULTS

The dielectric function $\varepsilon=\varepsilon_1+i\varepsilon_2$ of $LaFe_{0.5}Cr_{0.5}O_3$ at room temperature was obtained from ellipsometry measurements. Peaks in the imaginary part of the dielectric function

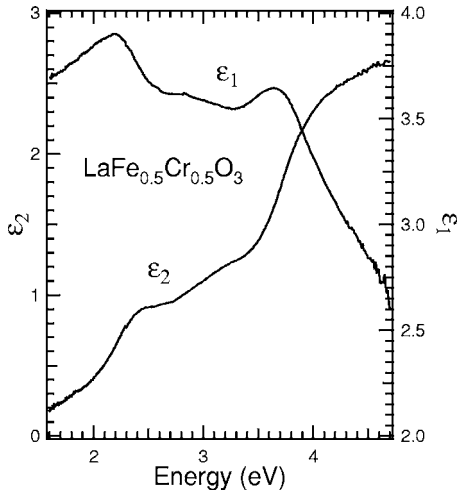

FIG. 2. The dielectric function $\varepsilon=\varepsilon_1+i\varepsilon_2$ at room temperature as a function of excitation energy. The imaginary part (ε_2) displays a clear peak at approximately 2.4 eV. The measurements were made on a polished sample of $LaFe_{0.5}Cr_{0.5}O_3$.

(ε_2) are related to the absorption processes in the material such as interband transitions and local interactions. The prominent peak in ε_2 at approximately 2.4 eV (Fig. 2) is of particular interest since it indicates an absorption process at this energy that can lead to resonance effects for $\lambda=515$ nm (2.41 eV incident energy) laser light.

Room-temperature (RT) Raman scattering using $\lambda=515$ nm (Fig. 3) reveals remarkable first and higher order features in the mixed *B*-site compounds ($x=0.1$, 0.5, and 0.9). In these compounds, the first order spectra ($E=\hbar\nu \lessapprox 800\ \mathrm{cm}^{-1}$) in parallel scattering configuration are dominated by an intense feature located around 700 cm^{-1} with additional first order modes present primarily in the 400 and 200 cm^{-1} energy regions (Fig. 3, inset). In accordance with studies on structurally related compounds,[20,26–29] we assign the 700 cm^{-1} peak to a symmetric oxygen breathing mode. In particular, we note that the modes with JT-like normal coordinates (Q_2+Q_3) always appear at lower energies in related compounds.[23,24,26]

At energies above the first order spectra ($E=\hbar\nu \gtrapprox 800\ \mathrm{cm}^{-1}$) in the mixed *B*-site compounds, exceptionally strong second and higher order scatterings are observed. The second order is located at an energy slightly lower than twice the energy of the first order mode (Fig. 3). Similar downshifts are seen for the third and four order peaks present at higher energies. Such downshifts are expected for higher order scattering and reflect the asymmetry of the anharmonic potential of the system.[12,30] The principal peaks display a slight asymmetry, reminiscent of a Fano profile indicating the presence of a coherent electron-phonon coupling. Further, the frequencies of the principal mode and corresponding higher order excitations increase with increasing Cr content in the $x=0.1$, 0.5, and 0.9 compounds. This hardening is likely to be caused by the contraction of the unit cell,[31] reflecting the increase in bond strength as Fe^{3+} is replaced by Cr^{3+}. In addition, the mass difference between Fe (55.8 g/mol) and Cr (52.0 g/mol) may cause a modulation in the system potential that also contributes to the energy

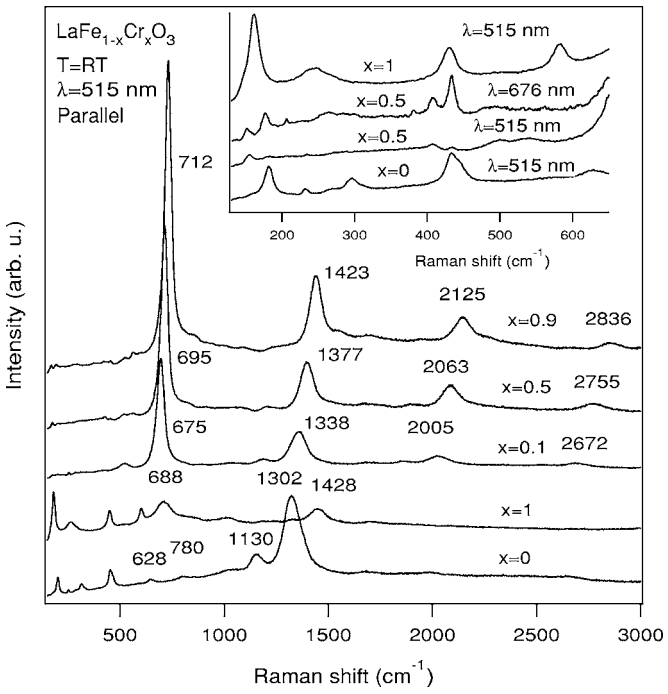

FIG. 3. Raman spectra of the isostructural compounds $LaFe_{1-x}Cr_xO_6$. Considerable higher order scattering appears in the compounds with both Fe and Cr present. Higher energy bands in the $x=0$ and $x=1$ compounds are believed to be of magnetic origin. Samples $x=0.9$ and $x=1$ are unoriented powders. The inset shows the low-energy region for $x=0$, 0.5, and 0.9 using $\lambda=515$ nm and $x=0.5$ using $\lambda=676$ nm.

shift. The similarity between the scattering from the $x=0.5$ compound, which is granular and focusing on specific planes is possible, and the $x=0.9$ compound, which is a fine powder and represents scattering from an average of unoriented samples, indicates that the average signal is strongly dominated by the scattering from the *ac* planes.

Below 600 cm^{-1}, the first order spectra of the unsubstituted compounds ($x=0$ and $x=1$) show qualitative similarities with the mixed *B*-site compounds in that the main activity is in the 200 and 400 cm^{-1} regions (Fig. 3, inset). The differences in the lower-energy part of the first order spectrum between the mixed and pure *B*-site compounds are likely to be caused by a small level of local ordering on the *B* site (too small to be detectable using neutron diffraction.) Such an ordering corresponds to a local lowering of symmetry from orthorhombic ($Pnma$) to monoclinic ($P2_1/n$) (Ref. 32) and should be associated with an activation of Raman modes in the low-energy spectral region.[29] The presence of local *B*-site order in $LaFe_{0.5}Cr_{0.5}O_3$ is also indicated by a weak uncompensated magnetic moment below T_N.[21]

In contrast to the samples with a mix of Fe and Cr ions on the *B* site, the compounds containing only Fe or Cr show no, or little, Raman activity in the 700 cm^{-1} energy region (Fig. 3). The low intensity of the first order breathing mode in the $x=0$ and $x=1$ compounds, as well the absence of the series of higher order excitations characteristic of the mixed *B*-site compounds, is related to the lack of an orbitally mediated electron-phonon coupling in $LaFeO_3$ and $LaCrO_3$. This subject is covered extensively in Sec. IV.

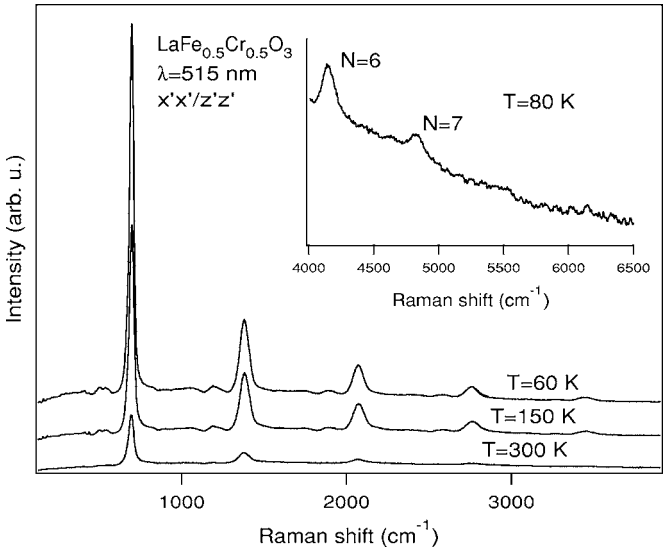

FIG. 4. First and higher order excitations in the compound $LaFe_{0.5}Cr_{0.5}O_3$ for temperatures $T=300$, 150, and 60 K. The inset shows the sixth, seventh, and a possible eighth order of the 700 cm^{-1} peak at $T=80$ K. Both the main figure and the inset show data collected using the $\lambda=515$ nm excitation wavelength and parallel $x'x'/z'z'$ scattering configuration.

At 80 K, modes up to seventh order are clearly distinguishable in $LaFe_{0.5}Cr_{0.5}O_3$ using $\lambda=514.5$ nm and parallel $x'x'(z'z')$ scattering configuration (Fig. 4). Further, the temperature study of the first and higher orders shows that the integrated intensity of the 700 cm^{-1} mode increases with decreasing temperature (Fig. 5, bottom), while the ratio between the integrated intensity (I) of the first (I_1) and higher (I_N) order excitations does not show any clear change with decreasing temperature. The median value of I_2/I_1 between 300 and 20 K is 0.54 (Fig. 5, bottom).

The polarization study of $LaFe_{0.5}Cr_{0.5}O_3$ (Fig. 6) reveals that the intensities of the higher orders observed in cross-polarized scattering configuration approaches those of the higher orders in parallel scattering configuration as N increases (Fig. 6), the integrated intensity of the second order excitation being 90% of the first order 700 cm^{-1} peak in cross-polarized $x'z'/z'x'$ scattering configuration (Fig. 5, top). This indicates that the higher orders are not subject to the strict selection rules of the principal excitation.

A strong feature at 700 cm^{-1} remains when the excitation energy is changed to 1.83 eV ($\lambda=676$ nm) (Fig. 7). This proves that this peak is an inelastic scattering feature and not a luminesence. However, the decrease in excitation energy also causes both the first order mode and the relative intensity of the second and first order excitations to decrease, showing the resonant character of both features (Fig. 7 and inset). For completeness, we present the effect of A-site substitution on the first and second order scatterings in the compound $La_{0.835}Sr_{0.165}Fe_{0.5}Cr_{0.5}O_{3-\delta}$. An exchange of La for Sr and the accompanying introduction of oxygen vacancies in the $x=0.5$ compound[22] cause a decrease in both the absolute integrated intensity of the first order peak and the relative intensity of the higher order peaks compared to the first order peak (Fig. 7). The cause of this effect is covered in Sec. IV.

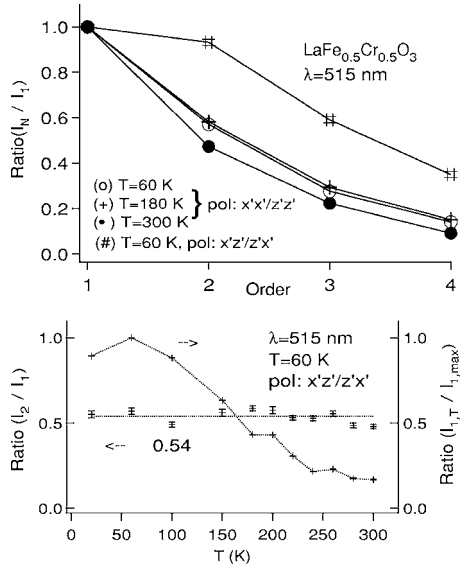

FIG. 5. Top shows the intensity ratio I_N/I_1 in $LaFe_{0.5}Cr_{0.5}O_3$ of the higher order excitations N at $T=300$, 180, and 60 K in parallel scattering configuration and at $T=60$ K in cross-polarized scattering configuration. Bottom shows the temperature dependence of the ratio between the second and first order excitation and the temperature dependence of the intensity of the principal excitation ($N=1$) compared to its maximum value at 60 K in $LaFe_{0.5}Cr_{0.5}O_3$. Error bars indicate errors associated with fitting the peaks to Lorentzian profiles.

The peaks at 1130 cm^{-1}, 1302 cm^{-1} in the $x=0$ compound, and 1428 cm^{-1} in the $x=1$ compound cannot be easily ascribed to second order scattering since the energies of these three bands do not represent approximately twice the energy of any first order mode. Furthermore, the first order phonon scattering in the 600–800 cm^{-1} region is very weak, particularly for the $x=0$ material, and their spectra reveal no clear features in the energy region where third and fourth order scatterings are expected (Fig. 3). The origin of these features is not yet clear but the observations of antiferromag-

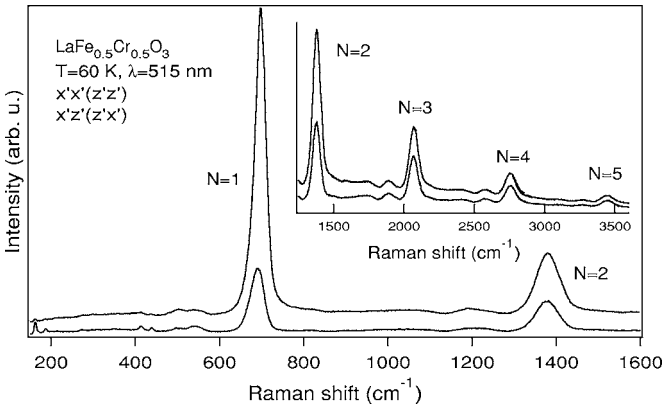

FIG. 6. Polarization dependence of the Raman spectra at $T=60$ K of the compound $LaFe_{0.5}Cr_{0.5}O_3$ for parallel $x'x'/z'z'$ and cross-polarized $x'z'/z'x'$ scattering configurations using $\lambda=515$ nm. The intensities of the higher orders in cross polarization approach those of parallel scattering configuration. Note, in particular, that the spectra in the inset are shown without offset.

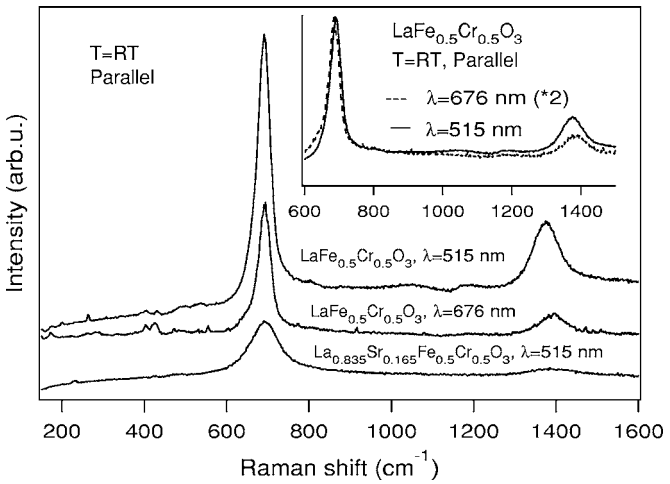

FIG. 7. First and second order excitations in $LaFe_{0.5}Cr_{0.5}O_3$ using $\lambda=515$ nm and $\lambda=676$ nm and the Sr-substituted compound $La_{0.835}Sr_{0.165}Fe_{0.5}Cr_{0.5}O_{3-\delta}$ using $\lambda=515$ nm. The inset shows the decrease in second order scattering compared with first order scattering when changing the laser energy from 2.41 ($\lambda=515$ nm) to 1.83 eV ($\lambda=676$ nm). The first order scattering using $\lambda=676$ nm is normalized to the first order scattering using $\lambda=515$ nm through a multiplication of the scattering intensity by a factor of 2.

netic (AFM) ordering around, or above, room temperature in $LaCrO_3$ ($T_N=282$ K) and $LaFeO_3$ ($T_N=750$ K) (Ref. 31) indicate that these modes may be of magnetic origin. Such an assignment is supported by the energy location of these modes. In a cubic G-type AFM, a nearest- neighbor spin-flip excitation (two magnon) corresponds to an energy increase of $5J$ (breaking of ten bonds), where J is the AFM coupling constant. For a two-magnon excitation in the 1300–1400 cm^{-1} region, this would yield $J\approx 33$ meV in line with the observed transition temperatures around or above room temperature[31] (i.e., $E\approx 1350$ $cm^{-1}\rightarrow J\approx 33$ meV $\rightarrow T_N\approx 390$ K). Further, the presence of two peaks in the energy region of magnetic scattering in $LaFeO_3$ may reflect the tilting of the spins away from the crystallographic a axis in this material.[33] According to neutron diffraction and magnetization data,[21] the $x=0.5$ sample exhibits a paramagnetic to AFM phase transitions with $T_N\approx 265$ K. However, using $\lambda=515$ nm, the energy region where two-magnon scattering would be expected is dominated by the second order scattering of the 700 cm^{-1} breathing mode obscuring the presence of a possible two magnon, also below T_N. The absence of dramatic effects in I_2/I_1 around T_N verifies the limited influence of the magnetic ordering on the scattering in the $x=0.5$ compound.

Further studies are needed to fully understand the intricate relations between the different degrees of freedom in the $LaFe_{1-x}Cr_xO_3$ system. In particular, the fact that the likely energy region for the two-magnon scattering coincides with the energy region for the strong second order scattering in the mixed B-site compounds clearly complicates the situation. A complete resonance study covering the visible and UV range (676.5–300 nm) as well as further measurements on compounds with low and high substitutional levels (less than 10% and more than 90%) are planned.

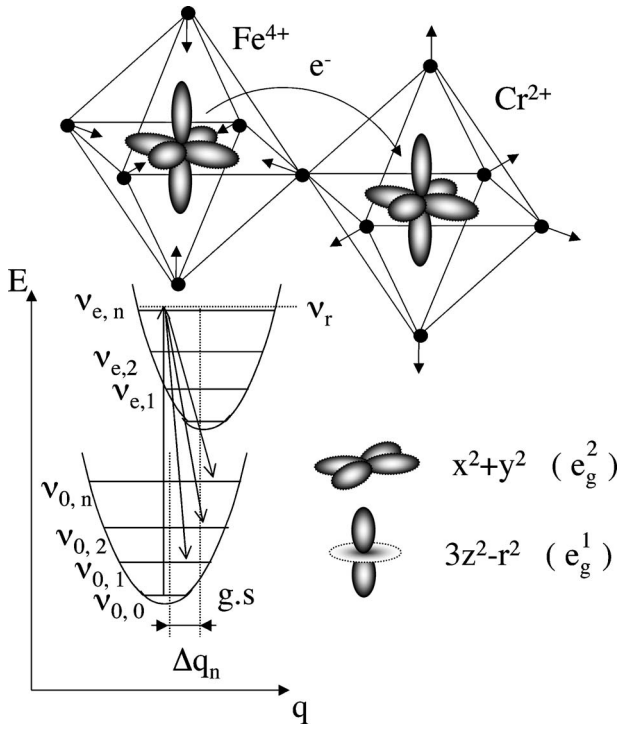

FIG. 8. A CT with an activation energy of 2.4 eV moves an electron from the Fe to the Cr ion. This leaves both the Fe and the Cr in the strongly coupling d^4 configuration with half-filled e_g bands causing a self-trapping mechanism of the oxygen octahedra (Δq_n). For the FC effect to be present for a vibrational mode with a normal coordinate q_n, the FC factor given by the overlap integral $\langle \nu_{0,f}|\nu_r\rangle\langle\nu_r|\nu_{0,i}\rangle$ must be nonzero. Here, the virtual state $|\nu_r\rangle$ of the Raman process must coincide with some vibrational state of the electronically excited state $|\nu_{e,n}\rangle$. The initial and final vibrational states of the Raman process ($|\nu_{0,i}\rangle$ and $|\nu_{0,f}\rangle$) are both in the electronic ground state.

IV. DISCUSSION

The intensity of a Stokes Raman scattering signal depends on the transition probability from the vibrational ground state to the final state, both in the electronic ground state, via a virtual state (Fig. 8, bottom left). A resonance may occur when this virtual state coincides with, or is close to, a vibrational level of an excited electronic state. Within the Born-Oppenheimer approximation, the electronic and vibrational states can be separated and in the case of a totally symmetric vibration, the essence of the resonance is captured by the Albrecht A term[12] containing the Franck-Condon factor given by the overlap of the wave functions of the vibrational states in the electronic ground and excited states (Fig. 8). For a resonance to occur, the FC factor must be nonzero and in the case of identical parabola, this is achieved by a shift in position between the parabola of the ground and excited electronic states. This shift is supplied by the trapping mechanism with a normal coordinate q_n (Fig. 8), causing the higher orders of the intrinsic mode with the same normal coordinate to go into resonance.[30]

In the cubic perovskite lattice, the presence of an octahedral crystal field splits the $3d$ level into a triply degenerate t_{2g}

level and a doubly degenerate e_g level.[4] Given the JT active d^4 and d^9 or low spin d^7 electronic configurations, the partly filled e_g band reflects a ground state with a static JT distortion of the oxygen octahedra. In a model with suppressed electron hopping, it has been shown that in the manganite $LaMnO_3$, the d^4 electron of the Mn^{3+} ion can move between the lower and upper e_g levels, creating an excited state with a flipped orbital through a localized electronic excitation (Frenkel exciton). This process couples to the oxygen lattice through the overlap between the *B*-site *d* and oxygen *p* orbitals, causing a self-trapping motion of the surrounding oxygen. This motion has a JT-like normal coordinate and increases the lifetime of the excited electronic state long enough for it to interact with the intrinsic phonon mode with a similar normal coordinate. The result is a FC process manifested by increased higher order scattering of, in particular, the JT-like phonon.[8,11,15,16]

In the $LaFe_{1-x}Cr_xO_3$ compounds, the electron configuration of the electronic ground state does not facilitate such an orbital- mediated electron-phonon coupling, since the $Fe^{3+}(d^5)$ and $Cr^{3+}(d^3)$ lack the strongly interacting half-filled e_g levels. However, based on the peak in ε_2 centered at 2.4 eV in the ellipsometry data (Fig. 2), we propose that a photon-mediated charge transfer takes place between neighboring Fe and Cr ions upon irradiation with the $\lambda=515$ nm (2.41 eV) laser. This process causes the presence of a distribution of $Fe^{4+}(d^4)Cr^{2+}(d^4)$ pairs in the strongly coupling d^4 configuration. The hypothesis of a charge transfer (CT) between the Fe and Cr is supported by partial density of state (PDOS) calculations, carried out for *B*-site-ordered DP La_2FeCrO_6 using generalized gradient approximation (GGA) and local-density approximation (LDA)+*U* methods.[34] These results indicate a complex interplay between the Fe and Cr electronic levels mediated by competing ferro- and ferrimagnetic superexchange processes. According to this work, the majority-spin (spin-up) Fe e_g band in the FiM ground state is located between −2 and −0.5 eV and the empty spin-down Cr e_g band between 0.5 and 1.5 eV. Thus, the energy gap between these bands is such that a CT from Fe to Cr can be induced by photons with energy around 2.4 eV. This process is directly manifested by the observed peak in this energy region in the ε_2 spectrum of the ellipsometry data (Fig. 2). We note that a CT energy of about 2.4 eV between Fe and Cr is in line with all cases studied in Ref. 34 (GGA and LDA+*U* calculations on FM and FiM ground states).

During the CT, the d^4 electrons in both Fe and Cr occupy a combination of the e_g^1 and e_g^2 levels and couple to all six surrounding oxygen ions through the corresponding combination of the z^2-r^2 and x^2+y^2 *d* orbitals. [The notation used here to label the orbitals is the standard notation representing *d* orbitals pointing from the TM *B* sites toward the oxygen sites along the crystallographic *a*, *b*, and *c* axes (Fig. 1).] This orbital coupling stabilizes the CT state long enough for the Fe^{4+}-Cr^{2+} electron configuration to interact with the lattice dynamics and couple to the intrinsic symmetric breathing mode in the oxygen lattice. The effect is a contraction of the oxygen octahedron surrounding the Fe^{4+} ion due to the different Coulomb forces in the CT state and a corresponding expansion of the adjacent octahedron surrounding the Cr^{2+} ion (Fig. 8, top). When the electron eventually transfers back to the Fe ion, the oxygen lattice relaxes back to its unperturbed state. Thus, the CT of an electron from the Fe^{3+} to the Cr^{3+} ion causes an orbital- mediated local symmetric breathing mode of A_g-like symmetry to act as the self-trapping motion.

To explain the exceptional intensities of the higher order scattering in the $x=0.1$, 0.5, and 0.9 compounds, we use the FC mechanism described above. According to group theory, a Raman-active oxygen breathing mode is intrinsic to the compound but is of B_{3g} symmetry in a perfect *Pnma* structure[23,24] and should not be activated in the *ac* plane. However, on the local scale where the CT takes place and the resonant dynamics occurs, the structure is likely to be influenced by local domains of *B*-site order, and hence the selection rules of the *Pnma* structure cannot be expected to hold strictly. The possibility of getting an activation of a breathing mode of A_g-like symmetry due to local effects is also indicated by recent reports of such modes in other mixed *B*-site perovskites.[27,28] Thus, the higher orders observed originate from the intrinsic breathing mode, Raman activated by local effects, and strongly enhanced by the FC effect.

This enhancement of the higher orders also enables us to comment on the different impact of the selection rules on the first and higher order scatterings. The principal mode has A_g-like symmetry and thus dominates the parallel scattering configuration. However, the higher order FC modes are not strictly subject to the selection rules of the first order excitations, and the intensities of the higher orders approach similar relative magnitudes in parallel and cross-polarized scattering configurations for large *N* (Fig. 6). Thus, the general view that the selection rules obtained from group theory concern primarily first order spectral features under nonresonant conditions and do not apply strictly to higher order excitations in the presence of resonance effects[30] is confirmed. Indeed, the first order selection rules appear to lose influence as *N* increases (Fig. 6). This behavior is qualitatively the same for all studied temperatures between RT and 20 K.

The introduction of Sr onto the *A* site of the material results in oxygen deficiency with an experimental value of $\delta=0.054$ for $x=0.165$.[22] With Sr substitution, the strong resonances present for $\lambda=514$ nm of the first and higher order excitations show a simultaneous significant decrease. The simplest explanation for this behavior would be that the resonance frequencies of these phenomena simply shift as Sr is introduced. However, we believe that the changes in the compound induced by Sr substitution cause a decrease in the actual resonances. We note that the nominal amount of vacancies associated with $x=0.165$ ($\delta_{nom}=0.0825$), based on simple charge balance arguments and oxidation states Fe^{3+} and Cr^{3+}, differs from the observed experimental value ($\delta_{expt}=0.054$). This discrepancy can be compensated by a number of Fe ions taking a 4+ oxidation state in order to retain electroneutrality. The presence of d^4 Fe ions indicates the possibility of a slight static distortion existing already in the electronic ground state. This situation corresponds to an increase in overlap between the ground state and the excited electronic state, resulting in a decrease of the efficiency of the self-trapping mechanism and hence the stability and lifetime of the self- trapped state. Such a decrease in lifetime

will diminish both I_1 and I_N/I_1. In addition, it is likely that the introduction of Sr ions and the accompanying oxygen vacancies also cause disruptions in the CT pathways necessary for electron mediation, causing a further decrease in the resonances.

In the literature, series of equidistant peaks are sometimes interpreted not as true Raman scattering but as hot luminescence.[35] However, it is predicted that the linewidth of the true Raman-scattering mode should be roughly proportional to the order of the scattering (N), while modes due to hot luminescence are predicted to decrease in width with N, being proportional to $(N_{max}-N)$, where N_{max} is the highest order observed.[35] From the steady increase in the linewidth of the observed excitations (Fig. 4), we conclude that the modes exhibited by La_2FeCrO_6 are true higher order Raman modes.

Finally, we note that a strong FC resonance could appear even if only a small fraction of the B-site ions are excited to the active d^4 configuration. Such series of higher order scattering due to minute amounts of impurities in the lattice matrix have previously been reported in CsI salts contaminated with MnO_4^{2-} inclusions.[36]

V. CONCLUSIONS

In the B-site-disordered perovskites $LaFe_{1-x}Cr_xO_3$, $x=0.1$, 0.5, and 0.9, an intense phonon mode around 700 cm^{-1} and strong multiphonon scattering are observed using $\lambda=515$ nm (2.41 eV). The presence of this first and higher order spectrum is dependent on the presence of both Fe and Cr mixed on the B site and does not appear in the $x=0$ and $x=1$ compounds. Based on ellipsometry data and electronic band-structure calculations,[34] we propose an explanation based on a CT from Fe to Cr ions. This activates an oxygen breathing mode of A_g-like symmetry through an orbital-mediated electron-lattice coupling and leads to a remarkable increase in higher order scattering through a FC process. The higher orders are seen to be at least $N=7$ at 80 K and are drastically enhanced due to the increased overlap to higher order vibrational levels caused by the shift of the excited state along the symmetric breathing normal coordinate as an effect of the coupling between the CT and the lattice.[37] This study establishes the presence of a strong electron-phonon interaction and a FC effect in the mixed B-site perovskites, and it introduces an interatomic CT mechanism as the electronic excitation with which the lattice interacts. In doing so, it indicates that the FC mechanism is a more common mechanism for higher order scattering in solids than previously believed. In particular, among the TM oxides, it is not limited to the JT-distorted, orbitally ordered, low doping manganites with suppressed hopping. Given the intense and relatively simple characteristics of the inelastic scattering features presented in this study, we believe that the $LaFe_{1-x}Cr_xO_3$ system is a suitable model system for research on the strong interactions between the electronic, structural, orbital, and possibly magnetic degrees of freedom in TM oxides as well as basic research on the FC mechanism in solids. Additional studies of the FC resonance in $LaFe_{1-x}Cr_xO_3$ can help us understand the nature of the strong electron-phonon coupling in these and similar materials.

ACKNOWLEDGMENTS

We are thankful to M. Bastjan for performing the ellipsometry measurements, A. Eriksson for samples and structural data, and I. Panas for helpful discussions. C.S.K. acknowledges support from the European Commission Sixth Framework Programme through the Marie Curie actions. The support of the Swedish Research Council and the Foundation for Strategic Research (Complex Oxide Programme) is gratefully acknowledged: DFG Ru 773/2-3 and HGF VH-FZ-007.

*Present address: Permascand AB, P.O. Box 42, SE-84010 Ljungaverk, Sweden.

†Present address: Department of Chemistry, University of St. Andrews, Fife, KY 16 9ST Scotland, United Kingdom.

‡Present address: Department of Environmental Inorganic Chemistry, Chalmers University of Technology, SE-412 96, Göteborg Sweden.

[1] J. Bednorz and K. A. Müller, Z. Phys. B: Condens. Matter **64**, 189 (1986).

[2] A. P. Ramirez, J. Phys.: Condens. Matter **9**, 8171 (1997).

[3] J.-H. Park, E. Vescovo, H.-J. Kim, C. Kwon, R. Ramesh, and T. Venkatesan, Nature (London) **392**, 794 (1998).

[4] A. J. Millis, Nature (London) **392**, 147 (1998).

[5] A. J. Millis, P. B. Littlewood, and B. I. Shraiman, Phys. Rev. Lett. **74**, 5144 (1995).

[6] A. J. Millis, B. I. Shraiman, and R. Mueller, Phys. Rev. Lett. **77**, 175 (1996).

[7] K.-I. Kobayashi, T. Kimura, H. Sawada, K. Terakura, and Y. Tokura, Nature (London) **395**, 677 (1998).

[8] P. B. Allen and V. Perebeinos, Phys. Rev. Lett. **83**, 4828 (1999).

[9] Jeroen van den Brink, Phys. Rev. Lett. **87**, 217202 (2001).

[10] P. B. Allen and V. Perebeinos, Nature (London) **410**, 155 (2001).

[11] V. Perebeinos and P. B. Allen, Phys. Rev. B **64**, 085118 (2001).

[12] K. Nakamoto, *Infrared and Raman Spectra of Inorganic and Coordination Compounds*, 5th ed. (Wiley, New York, 1997), Pt. A.

[13] E. Saitho, S. Okamoto, K. T. Takahashi, K. Tobe, K. Yamamoto, T. Kimura, S. Ishihara, S. Maekawa, and Y. Tokura, Nature (London) **410**, 180 (2001).

[14] M. Grüninger, R. Rückamp, M. Windt, P. Reutler, C. Zobel, T. Lorenz, A. Freimuth, and A. Revcolevschi, Nature (London) **418**, 39 (2001).

[15] L. Martín-Carrón and A. de Andrés, Phys. Rev. Lett. **92**, 175501 (2004).

[16] R. Krüger, B. Schulz, S. Naler, R. Rauer, D. Budelmann, J. Bäckström, K. H. Kim, S.-W. Cheong, V. Perebeinos, and M. Rübhausen, Phys. Rev. Lett. **92**, 097203 (2004).

[17] K.-Y. Choi, P. Lemmens, G. Güntherodt, Yu. G. Pashkevich, V. P. Gnezdilov, P. Reutler, L. Pinsard-Gaudart, B. Büchner, and A.

Revcolevschi, Phys. Rev. B **72**, 024301 (2005).
[18] K.-Y. Choi, Yu. G. Pashkevich, V. P. Gnezdilov, G. Güntherodt, A. V. Yeremenko, D. A. Nabok, V. I. Kamenev, S. N. Barilo, S. V. Shiryaev, A. G. Soldatov, and P. Lemmens, Phys. Rev. B **74**, 064406 (2006).
[19] A. E. Pantoja, H. J. Trodahl, A. Fainstein, R. G. Pregliasco, R. G. Buckley, G. Balakrishnan, M. R. Lees, and D. McK. Paul, Phys. Rev. B **63**, 132406 (2001).
[20] Y. Fujioka, J. Frantti, and M. Kakahani, J. Phys. Chem. B **108**, 17012 (2004).
[21] A. K. Azad, A. Mellergård, S.-G. Eriksson, S. A. Ivanov, S. M. Yunus, F. Lindberg, G. Svensson, and R. Mathieu, Mater. Res. Bull. **40**, 1633 (2005).
[22] A. K. Azad and S.-G. Eriksson (unpublished).
[23] M. N. Iliev, M. V. Abrashev, H.-G. Lee, V. N. Popov, Y. Y. Sun, C. Thomsen, R. L. Meng, and C. W. Chu, Phys. Rev. B **57**, 2872 (1998).
[24] M. V. Abrashev, J. Bäckström, L. Börjesson, V. N. Popov, R. A. Chakalov, N. Kolev, R.-L. Meng, and M. N. Iliev, Phys. Rev. B **65**, 184301 (2002).
[25] L. Martín-Carrón and A. de Andrés, Eur. Phys. J. B **22**, 11 (2001).
[26] A. Ishikawa, J. Nohara, and S. Sugai, Phys. Rev. Lett. **93**, 136401 (2004).
[27] A. G. Souza Filho, J. L. B. Faria, I. Guedes, J. M. Sasaki, P. T. C. Freire, J. Mendes Filho, M. M. Xavier, Jr., F. A. O. Cabral, J. H. de Araújo, and J. A. P. da Costa, Phys. Rev. B **67**, 052405 (2003).
[28] A. Dubroka, J. Humliicek, M. V. Abrashev, Z. V. Popovic, F. Sapina, and A. Cantarero, Phys. Rev. B **73**, 224401 (2006).
[29] Y. Fujioka, J. Frantti, and M. Kakihana, J. Phys. Chem. B **110**, 777 (2006).
[30] *Handbook of Vibrational Spectroscopy*, edited by J. M. Chalmers and P. R. Griffiths (Wiley, New York, 2002), Vol. 1.
[31] A. Belayachi, E. Loudghiri, M. El Yamani, M. Nouges, J. L. Dormann, and M. Taibi, Ann. Chim. (Paris) **23**, 297 (1998).
[32] P. M. Woodward, Acta Crystallogr., Sect. B: Struct. Sci. **53**, 32 (1997).
[33] T. Pererlin-Neumaier and S. Steichele, J. Magn. Magn. Mater. **59**, 351 (1986).
[34] K. Miura and K. Terakura, Phys. Rev. B **63**, 104402 (2001).
[35] T. P. Martin, Phys. Rev. B **13**, 3617 (1975).
[36] T. P. Martin and S. Onari, Phys. Rev. B **15**, 1039 (1977).
[37] J. Kanamori, J. Appl. Phys. **31**, 14S (1960).